Chinese Journal of Catalysis 37 (2016) 1569–1577

available at www.sciencedirect.com

ScienceDirect

journal homepage: www.elsevier.com/locate/chnjc

Article

Chemoselective transfer hydrogenation to nitroarenes mediated by oxygen-implanted MoS_2

Chaofeng Zhang [a,b], Xu Wang [c], Mingrun Li [a], Zhixin Zhang [a], Yehong Wang [a], Rui Si [c], Feng Wang [a,*]

[a] *State Key Laboratory of Catalysis, Dalian National Laboratory for Clean Energy, Dalian Institute of Chemical Physics, Chinese Academy of Sciences, Dalian 116023, Liaoning, China*

[b] *University of Chinese Academy of Sciences, Beijing 100049, China*

[c] *Shanghai Synchrotron Radiation Facility, Shanghai Institute of Applied Physics, Chinese Academy of Sciences, Shanghai 201204, China*

ARTICLE INFO

Article history:
Received 3 June 2016
Accepted 11 July 2016
Published 5 September 2016

Keywords:
MoS_2
Coordinative unsaturated Mo
Nitroarene
Transfer hydrogenation
Formate
Heterogeneous catalysis

ABSTRACT

We present an efficient approach for the chemoselective synthesis of arylamines from nitroarenes and formate over an oxygen-implanted MoS_2 catalyst (O-MoS_2). O-MoS_2 was prepared by incomplete sulfidation and reduction of an ammonium molybdate precursor. A number of Mo–O bonds were implanted in the as-synthesized ultrathin O-MoS_2 nanosheets. As a consequence of the different coordination geometries of O (MoO_2) and S (MoS_2), and lengths of the Mo–O and Mo–S bonds, the implanted Mo–O bonds induced obvious defects and more coordinatively unsaturated (CUS) Mo sites in O-MoS_2, as confirmed by X-ray diffraction, Raman spectroscopy, X-ray photoelectron spectroscopy, high resolution transmission electron microscopy, and extended X-ray absorption fine structure characterization of various MoS_2-based materials. O-MoS_2 with abundant CUS Mo sites was found to efficiently catalyze the chemoselective reduction of nitroarenes to arylamines.

1. Introduction

Functionalized arylamines [1–3] and their derivatives, such as imines and aromatic azo compounds [4,5], are widely used for the synthesis of dyes, pigments, agrochemicals, pharmaceuticals pesticides, herbicides, and other fine chemicals [6]. Previous studies on the reduction of nitroarenes to anilines have been mainly focused on supported catalysts containing d_6–d_{10} noble metals and active Ni-based catalysts [7–13]. A crucial issue for the general application of these heterogeneous catalysts for nitro reduction is their selectivity. Different methods, including metal particle size tailoring [14–16], use of alloy nanoparticles [17–19], metal-support cooperative effect regulation [20–22], and solvent and additive screening, have been employed to promote catalyst selectivity. Taking into account the complex synthesis and oxidizable nature of these noble metal catalysts, there is a strong incentive to develop nitroarene reduction processes with efficient and robust catalysts based on non-precious metals [23–30], which can catalyze the reaction in less harmful solvents and do not require many additives.

Compared with catalytic hydrogenation using H_2 as the hydrogen source, the convenient and selective transfer hydrogenation process has drawn much attention. As an important hydrogen storage process [31,32], transfer hydrogenation using formic acid provides an attractive alternative to the catalytic hydrogenation of nitroarenes; however, few active heterogeneous catalysts based on non-precious metals have been

* Corresponding author. Tel/Fax: +86-411-84379762; E-mail: wangfeng@dicp.ac.cn
This work was supported by the National Natural Science Foundation of China (21422308, 21403216, 21273231) and Dalian Excellent Youth Foundation (2014J11JH126).
DOI: 10.1016/S1872-2067(16)62504-4 | http://www.sciencedirect.com/science/journal/18722067 | Chin. J. Catal., Vol. 37, No. 9, September 2016

reported [33–35].

For the reduction of nitroarenes with formate, Llusar and co-workers [36] confirmed that coordinative unsaturated (CUS) Mo sites in cubane-type $[Mo_3S_4X_3(dmpe)_3]^+$ clusters played a crucial role in the transformation of formate to the active hydrogen species for nitroarene reduction. Taking into account the similar structural skeleton of $[Mo_3S_4X_3(dmpe)_3]^+$ clusters and MoS_2, we postulate that MoS_2 could be a robust and easily prepared catalyst for reduction reactions. However, it has been both theoretically and experimentally proved that while the edge sites of MoS_2 that have CUS Mo sites are catalytically active, the mostly exposed basal planes are inactive [37–39]. Chemical and mechanical exfoliation methods can increase the number of active sites [40–42]. Therefore, in light of the high-aspect-ratio architecture of MoS_2 nanosheets, a novel strategy should be developed to change the mostly exposed MoS_2 basal planes to be catalytically active.

It is anticipated that the fractional replacement of S with O in the MoS_2 crystalline lattice may create extra CUS Mo sites because the ligand geometries of O (MoO_2) and S (MoS_2), and the lengths of the Mo–O and Mo–S bonds are remarkably different [43,44], which could induce lattice distortion and defects. However, it is rather challenging to obtain such a structure via post-modification, because perfect MoS_2 basal planes consisting of closed shell Mo centers and strong Mo–S bonds can either endure post-modification or will be completely changed. Therefore, one possible way to implant O into the MoS_2 lattice should be via bulk synthesis.

Encouraged by previous studies of MoS_2 in photonic and electrocatalytic applications [45–48], we successfully synthesized oxygen-implanted MoS_2 (designated as O-MoS_2) via incomplete sulfidation and reduction of a molybdate precursor ($[Mo_7O_{24}]^{6-}$). The presence of deliberately left Mo–O or Mo=O bonds in the O-MoS_2 lattice was confirmed by XPS and Raman spectroscopy characterization. HRTEM observations revealed that the as-synthesized O-MoS_2 had a coiled nanosheet morphology with highly distorted crystal lattice and defect-rich zones on its basal planes. EXAFS indicated the existence of four-fold and five-fold CUS Mo sites. As a result of the lattice defects, abundant active CUS Mo sites existed in the O-MoS_2, which functioned as active sites in the hydrogen transfer reduction of nitroarenes with formate in water.

2. Experimental

2.1. Materials

All chemicals were of analytical grade and used as obtained without further purification.

2.2. Catalyst preparation

The preparation of the O-MoS_2 was adapted from Xie et al [46]. Typically, 3.70 g $(NH_4)_6Mo_7O_{24}\cdot 4H_2O$ (3 mmol, AHM) and 6.85 g thiourea (90 mmol) were dissolved in 105 mL distilled water and placed in an autoclave. The autoclave was tightly sealed in air and then placed in an oven thermally stabilized at 180 °C for 24 h, after which the autoclave was removed from the oven and allowed to naturally cool to room temperature. The solid product was centrifuged, washed with distilled water and ethanol, and then dried at 60 °C under vacuum. The final dry solid was O-MoS_2. O-MoS_2-Ar was also prepared by treating O-MoS_2 in an Ar flow at 250 °C for 3 h.

The chemical exfoliation of commercial 2H-MoS_2 (designated as ceMoS_2) was adapted from Chou et al [49]. 700 mg of 2H-MoS_2 powder was immersed in 10 mL of *n*-butyllithium (1.6 mol/L in hexane) and stirred for 48 h under Ar protection. After the stirring, 20 mL hexane was added to the mixture, and 0.36 mL H_2O was then added dropwise over 10 min under Ar flow. After 0.5 h, a further 200 mL of H_2O was added to the mixture. The mixture was then sonicated for 2 h to achieve exfoliation. The ceMoS_2 nanosheets were then centrifuged and washed with water and ethanol five times, and the final products were obtained after vacuum drying at room temperature.

MoO_3/2H-MoS_2 (MoO_3, 5 wt%) was prepared by impregnating 2H-MoS_2 (1.0 g) in 8 mL of AHM solution (61 mg). The extra solvent was evaporated on a metal heating plate at 120 °C. The obtained dry solid was then annealed at 500 °C for 2 h in Ar flow (30 mL/min). MoO_2/2H-MoS_2 (MoO_2, 5 wt%) was obtained by adding 2H-MoS_2 (1.0 g) to 8 mL of phosphomolybdic acid solution (7.5 g/L). The extra solvent was evaporated on a metal heating plate at 120 °C. The obtained dry solid was then reduced at 500 °C for 2 h in a H_2/N_2 (1/9) flow (30 mL/min) [28]. Partially oxidized 2H-MoS_2 (2H-MoS_2-O_2) was prepared by treating 2H-MoS_2 in an air flow (30 mL/min) at 400 °C for 0.5 h.

2.3. Characterization

X-ray diffraction (XRD) analyses were conducted on a Rigaku D/Max 3400 powder diffraction system with Cu K_α radiation (λ = 1.542 Å). X-ray photoelectron spectroscopy (XPS) measurements were carried out on a VGESCALAB MK2 spectrometer equipped with an Al K_α X-ray source ($h\upsilon$ = 1486.6 eV) operated at a voltage of 12.5 kV. The binding energy (BE) was calibrated with the C 1*s* signal (284.6 eV) as a reference. Raman spectra were recorded on a micro-Raman spectrometer (Renishaw) equipped with a CCD detector using a He/Ne laser with a wavelength of 532 nm. High-resolution transmission electron microscopy (HRTEM) was carried out on an FEI Tecnai F30 electron microscope at an accelerating voltage of 300 kV.

X-ray absorption fine structure (XAFS) spectral measurements at the Mo K-edge (E_0 = 20000 eV) were performed at beamline BL14W1 of the Shanghai Synchrotron Radiation Facility (SSRF) operated at 3.5 GeV under "top-up" mode with a constant current of 240 mA. The XAFS data were recorded under transmission mode with ion chambers. The energy was calibrated according to the absorption edge of pure Mo foil. Athena and Artemis codes were used to extract the data and fit the profiles. For the X-ray absorption near edge structure (XANES) part, the experimental absorption coefficients as function of energy $\mu(E)$ were processed using background subtraction and normalization procedures, and are reported as "normalized absorptions". For the extended X-ray absorption fine

structure (EXAFS) part, the Fourier transformed (FT) data in *R* space were analyzed by applying a MoS_2 model for the Mo–S or Mo–Mo shell. The passive electron factors, S_0^2, were determined by fitting the experimental Mo foil data and fixing the Mo–Mo coordination number (CN) as 8+6, then fixed for further analysis of the investigated samples. The parameters describing the electronic properties (e.g., correction to the photoelectron energy origin, E_0) and local structural environment, including CN, bond distance (R), and Debye Waller (D.W.) factor around the absorbing atoms, were allowed to vary during the fitting process.

The CUS Mo sites of MoS_2 were probed and quantitatively analyzed by temperature-programmed desorption of ammonia (NH_3-TPD). A few milligrams of MoS_2 sample were loaded into a quartz tubular reactor, which was heated in a vertical electronic furnace. The desorption gas mixture was analyzed with an online mass spectrometer (THERMO^{Star} gas analysis system). The sample was initially pretreated at 100 °C under an Ar gas flow (30 mL/min) for 1 h to remove adsorbed impurities, and then cooled to room temperature. The flow gas was then switched to ammonia gas (99.9%) for 30 min at room temperature, and then back to Ar gas. The reactor temperature was increased to 400 °C at a ramp rate of 10 °C/min. An m/z = 17 signal was recorded for NH_3 and HO* from H_2O. The pure NH_3 mass signal was the value obtained after subtraction of the HO* mass signal from the m/z = 17 (NH_3 and HO*) signal, based on the reference mass spectrum of H_2O (m/z = 18). The quantitative results were calculated by referring to an ammonia standard curve.

2.4. Catalytic reactions and product analyses

For the catalytic reactions, typically, 0.5 mmol nitroarene, 2.5 mL solvent, 189 mg ammonium formate (3.0 mmol), and catalyst (20 mg) were added to a 15 mL pressure bottle reactor (maximum pressure 1.0 MPa, the typical reaction pressure was less than 0.4 MPa) with magnetic stirring. The atmosphere in the reactor was then replaced with Ar gas three times and tightly sealed. The reactor was placed in an oil bath preheated to the desired temperature. After the set reaction time, the reactor was quenched with cold water and the reaction mixture was diluted with 7.5 mL ethanol. The ethanol solution was analyzed by GC and GC-MS.

3. Results and discussion

3.1. General characterization

Two distinct peaks were observed at the low-angle region of the XRD pattern of the synthesized O-MoS_2, with *d*-spacings of 9.52 Å and 4.76 Å, respectively (Figure 1), indicating the formation of a new lamellar structure with enlarged interlayer spacing. Thermal treatment of O-MoS_2 in Ar gas at 250 °C for 3 h caused the XRD pattern of the material (O-MoS_2-Ar) to resemble that of commercial 2H-MoS_2 (JCPDS Card No. 37-1492), signifying that the thermal treatment transformed the O-MoS_2. It should be noted that no molybdenum oxide (MoO_2 or MoO_3)

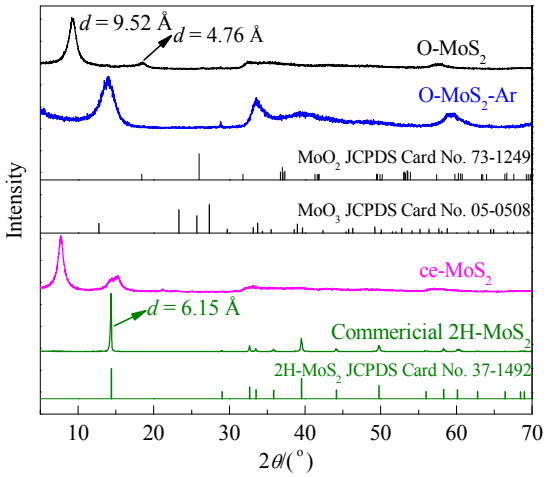

Fig. 1. XRD patterns of the MoS_2 materials.

crystallites were present in O-MoS_2 according to the XRD results. EDX analysis showed that the O content of the O-MoS_2 was 3.7 atom%. The TPD-MS results (Figure 2) showed that no lattice oxygen species were released from the O-MoS_2 as O_2 or SO_2 in the Ar flow below 250 °C.

XPS was carried out to investigate the chemical composition of the sample. As shown in Figure 3(a), two characteristic peaks arising from Mo $3d_{5/2}$ and Mo $3d_{3/2}$ orbitals were located at 229.1 and 232.2 eV in the spectra, respectively, suggesting the dominance of $Mo^{(IV)}$ in the product [39]. In contrast, the S 2*p* region (Figure 3(b)) primarily exhibited a single doublet with a $2p_{3/2}$ peak at 161.7 eV, which is consistent with −2 oxidation state of sulfur [39]. Furthermore, as shown in Figure 3(c), the observed O 1*s* peak located at 530.7 eV corresponded to the bonding of oxygen with Mo ions [50], suggesting the existence of $Mo^{(IV)}$–O bonds and thus verifying the successful incorporation of oxygen. The peak located at 532.0 eV can be attributed to adsorbed water. Because the molybdate precursor contained Mo^{6+}, it is very reasonable that the sulfidation and reduction process was incomplete and some Mo–O bonds remained in the O-MoS_2 sample.

More bonding information was revealed by the Raman spectra (Figure 4). The peaks at 376 and 401 cm^{-1} arose from

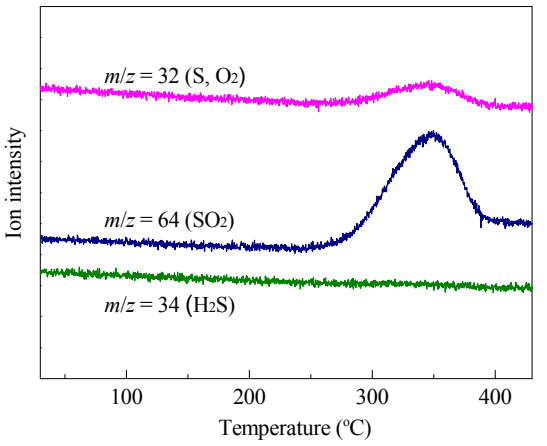

Fig. 2. TPD profiles of the O-MoS_2 in Ar flow.

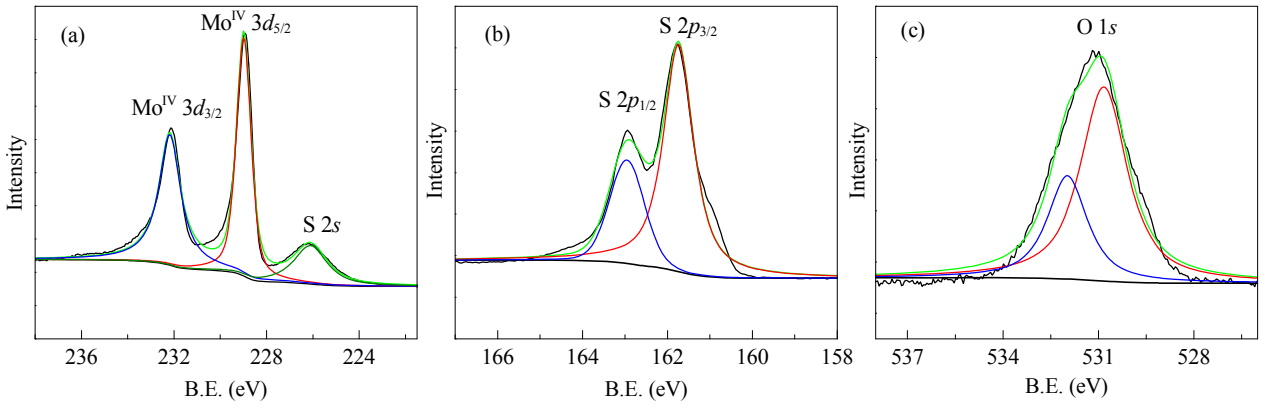

Fig. 3. XPS spectra showing the binding energy of molybdenum (a), sulfur (b), and oxygen (c) in the O-MoS_2.

the E^1_{2g} and A_{1g} vibrational modes of the Mo–S bonds, respectively, which are present in both 2H-MoS_2 and O-MoS_2 [51,52]. The peaks at 281 and 335 cm^{-1}, attributed to the B_{2g} and B_{1g} vibrational modes of δ(Mo=O) and δ(OMo_3) respectively, only present in O-MoS_2 [53]. Together with the peak at 662 cm^{-1} (OMo_3 units) and strong bands at 818 cm^{-1} (Mo–O–Mo bonds) and 993 cm^{-1} [ν(Mo=O)] [53], these results confirm that Mo–O bonds existed in O-MoS_2 with bonding types of Mo=O, OMo_3, and Mo–O–Mo. No MoO_2 phase appeared in the XRD pattern of the O-MoS_2, which implied a high dispersion of oxygen ions in the O-MoS_2 structure.

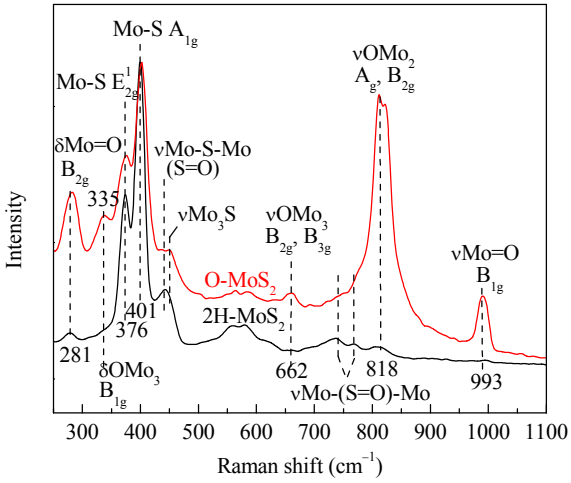

Fig. 4. Raman spectra of O-MoS_2 and 2H-MoS_2.

The morphology of the MoS_2 materials was observed by HRTEM. Both 2H-MoS_2 (Figure 5(b)) and ceMoS_2 (Figure 5(d)) preferentially exposed basal planes with ordered Mo and S atoms, indicating a well-crystallized phase. In contrast, O-MoS_2 featured twisted ultrathin sheets, the atomic surface of which was short-range ordered but long-range disordered, as illustrated by the high-resolution image shown in Figure 5(f). Except for the lattice-distorted zones, a number of subnano-sized defected zones with additional edge sites were also observed on O-MoS_2. The thermal treatment of O-MoS_2 in Ar flow at 250 °C reformed the O-MoS_2, and consequently, the O-MoS_2-Ar surface became ordered (Figure 5(h)).

Different from XRD, which is used to determine the crystal structure of well-crystallized materials, XAFS is very effective for determining the short-range local structure of heterogeneous catalysts [54–56]. As shown in Figure 5, O-MoS_2 was

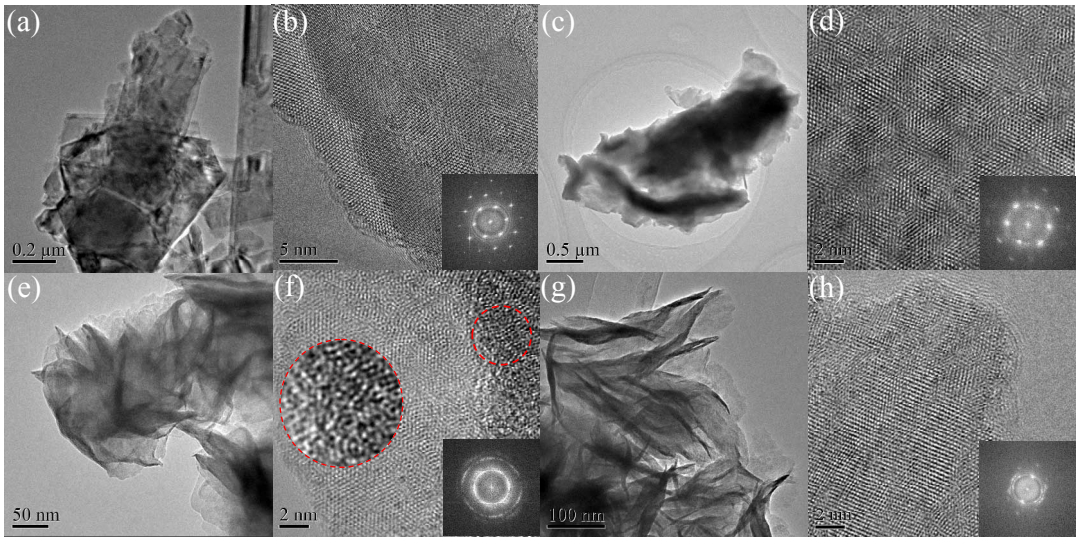

Fig. 5. TEM and HRTEM images of 2H-MoS_2 (a, b), ceMoS_2 (c, d), O-MoS_2 (e, f), and O-MoS_2-Ar (g, h).

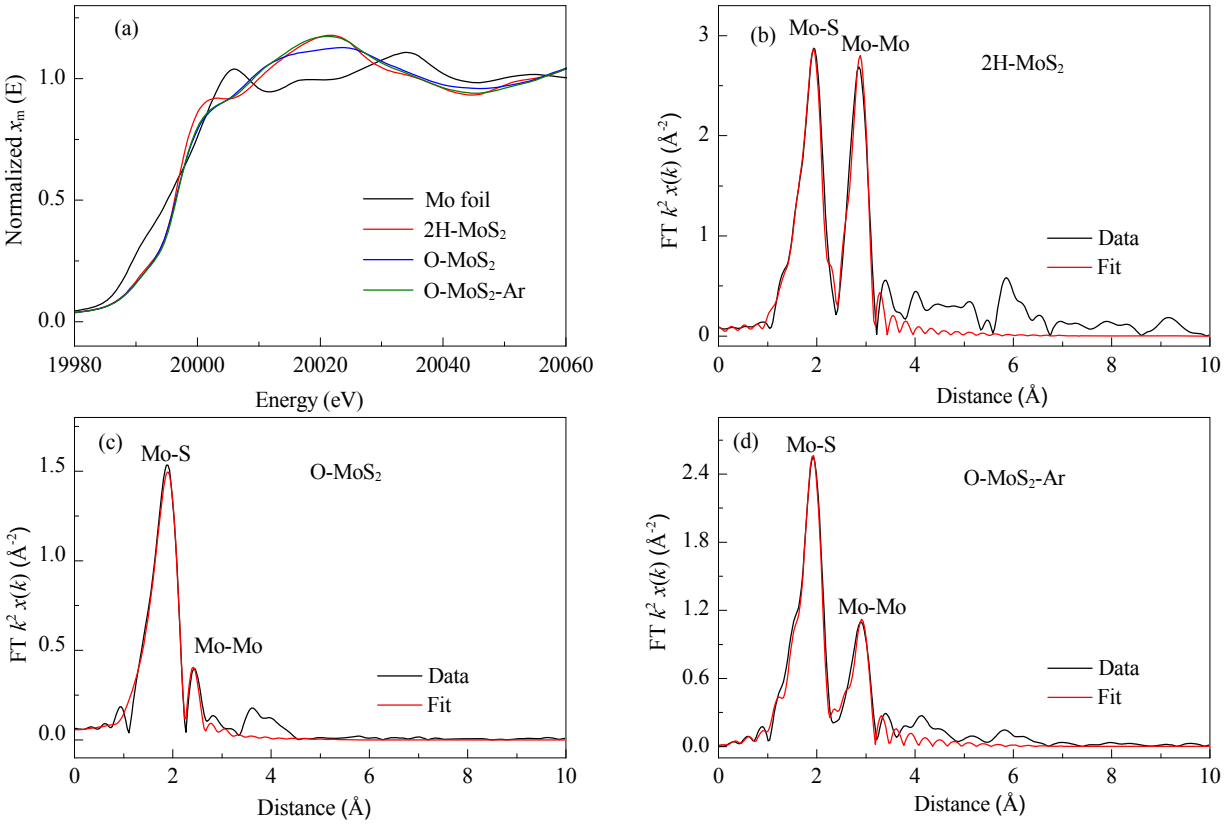

Fig. 6. Normalized E space spectra (a) of the Mo-based materials and EXAFS R space spectra of 2H-MoS_2 (b), O-MoS_2 (c), and O-MoS_2-Ar (d).

short-range ordered but long-range disordered. To obtain more structural information about the MoS_2-based materials, the EXAFS fitting method was adopted to evaluate the change in the coordination shell of the Mo atoms in the O-MoS_2 crystal structure.

It can be seen from Figure 6(a) that the Mo in all analyzed samples (2H-MoS_2, O-MoS_2, O-MoS_2-Ar) was more oxidized than Mo foil (Mo^0), which is in good agreement with the MoS_2 model. For the EXAFS part, Table 1 shows that the Mo–Mo distance (R) in the structure of 2H-MoS_2 was 3.17 Å, with a coordination number (CN) of 6.9±1.3, which are very close to the theoretical values ($R_{Mo\text{-}Mo}$ = 3.15 Å, $CN_{Mo\text{-}Mo}$ = 6) and show that the commercial 2H-MoS_2 had a well-crystallized phase. However, when oxygen (3.7 atom% according to the EDX results) was implanted into the MoS_2 structure via the hydrothermal synthesis method, the Mo–Mo distance decreased from 3.15 Å to 2.77 Å. This shows that the layered structure changed essentially, which was reflected by the differences in the XRD patterns of O-MoS_2 and 2H-MoS_2. The CN of Mo–Mo in O-MoS_2 changed more obviously to 0.6±0.2, which indicates that the Mo–Mo structure on the second shell almost disappeared and that O-MoS_2 had a high degree of disorder, as confirmed by HRTEM (Figure 5(f)). When O-MoS_2 was treated in Ar at 250 °C, the Mo–Mo distance in the resulting O-MoS_2-Ar returned to 3.16±0.01 Å, which showed that the thermal treatment not only reformed the interlayer spacing (Figure 1, O-MoS_2 and O-MoS_2-Ar) but also increased the crystallinity of the layer structure. Meanwhile, the CN of Mo–Mo in O-MoS_2-Ar was 2.9±1.1, which also indicated the existence of structural disorder. In the MoS_2-based materials, the Mo–S distance almost conformed to the theoretical value (Mo–S bond, 2.41 Å), and the CN of the Mo–S structure in each material was 4.2–5.2 with a lower fluctuation than that of the Mo–Mo structure. These results show that the interaction between Mo and S in the present system was strong and stable. Given that the oxygen content of the O-MoS_2 was almost ~3 atom% (EDX results) and the CN was 4.2±0.5 for the Mo–S structure and 0.6±0.2 for the Mo-Mo structure in O-MoS_2, O-MoS_2 was expected to contain more CUS Mo sites than 2H-MoS_2 or O-MoS_2-Ar. These CUS Mo sites were thought to exist as four-fold and five-fold coordinated Mo species.

Table 1
EXAFS fitting results of Mo-based catalysts.

Sample	Mo–S		Mo–Mo	
	R/Å	CN	R/Å	CN
Mo foil	—	—	2.72±0.00	8
			3.14±0.01	6
2H-MoS_2	2.40±0.00	5.2±0.5	3.17±0.00	6.9±1.3
O-MoS_2	2.41±0.01	4.2±0.5	2.77±0.02	0.6±0.2
O-MoS_2-Ar	2.40±0.01	4.7±0.4	3.16±0.01	2.9±1.1

R–Distance; CN–Coordination number.

3.2. *Probe catalytic reactions for the CUS Mo sites*

The reduction of nitrobenzene with ammonium formate ($HCOONH_4$) was used as a probe reaction to examine the

Table 2
Reduction of nitrobenzene to aniline [a].

Entry	Catalyst	Solvent	GC yield of aniline [g] (%)
1	2H-MoS_2	H_2O	<0.5
2	MoS_3	H_2O	4.1
3	ceMoS_2	H_2O	54.9
4	O-MoS_2	H_2O	>99
5	no catalyst	H_2O	<0.5
6 [b]	O-MoS_2	H_2O	0
7 [c]	O-MoS_2	H_2O	<0.5
8	O-MoS_2	ethanol	11.7
9	O-MoS_2	DMF	14.2
10	O-MoS_2	DMSO	82.0
11	MoO_2	H_2O	0
12	MoO_3	H_2O	0
13	MoO_3/2H-MoS_2	H_2O	0
14	MoO_2/2H-MoS_2	H_2O	0
15	O-MoS_2-Ar	H_2O	0.9
16	2H-MoS_2-O_2	H_2O	0
17 [d]	O-MoS_2	H_2O	76.1
18 [e]	no	H_2O	76.2
19	O-MoS_2 [f]	H_2O	>99

[a] Reaction conditions: nitrobenzene 0.5 mmol, $HCOONH_4$ 3.0 mmol, H_2O 2.5 mL, catalyst 20 mg, Ar, 130 °C, 3 h. [b] Without $HCOONH_4$. [c] $P(H_2)$ 0.4 MPa. [d] 1 h. [e] Hot filtration experiment for another 100-min reaction after 1 h reaction. [f] Reuse of O-MoS_2 for the fourth time. [g] Aniline was the only product.

change in the CUS Mo sites in the different MoS_2 materials [36]. The nitrobenzene conversion over 2H-MoS_2 and MoS_3 was 0.5% and 4.1%, respectively (Table 2, entries 1 and 2). Reaction over ceMoS_2 offered a 54.9% aniline yield (entry 3). Unexpectedly, reaction over O-MoS_2 gave >99% aniline yield within 3 h (entry 4). Both O-MoS_2 and $HCOONH_4$ were indispensable for the reaction (entries 5 and 6). Reaction with H_2 as reductant gave no product (entry 7), which implies that the reduction involves active hydrogen species from $HCOONH_4$, not molecular H_2. Water was the best solvent among water, ethanol, DMF, and DMSO (entries 8–10). This could be because $HCOONH_4$ was best ionized in water, which is regarded as the key step during the dehydrogenation of formate to the active H* species [36,57].

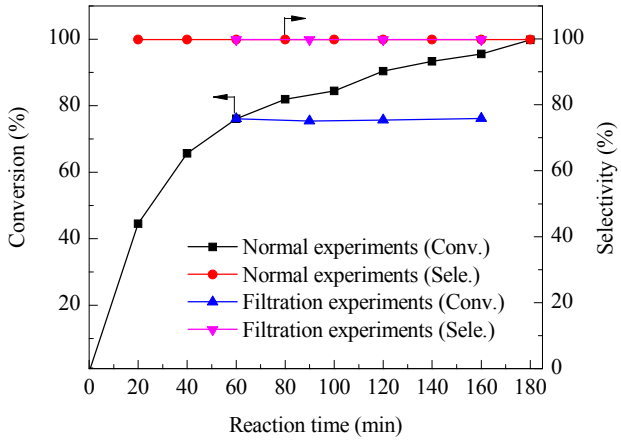

Fig. 7. Reduction of nitrobenzene with $HCOONH_4$. Reaction conditions: nitrobenzene 0.5 mmol, $HCOONH_4$ 3.0 mmol, H_2O 2.5 mL, O-MoS_2 20 mg 130 °C, Ar.

Some other Mo-based catalysts were compared with O-MoS_2. Pure MoO_2 and MoO_3 were inactive for nitrobenzene reduction (Table 2, entries 11 and 12). Even the highly dispersed molybdenum oxides on the 2H-MoS_2 support have no activity at all (entries 13 and 14). Thermal treatment in Ar made O-MoS_2 inactive (entry 15). An attempt to post-oxidize the perfect 2H-MoS_2 surface failed to obtain an active catalyst (entry 16), indicating the uniqueness of the present incomplete sulfidation and reduction process during the O-containing MoS_2 bulk synthesis. Catalyst hot filtration was also performed (entry 17). No further conversion occurred after the filtration over the next 100 min of reaction at 130 °C (entry 18), which indicated that the reaction was a heterogeneous catalysis (Figure 7). The spent catalyst was filtered out, washed with ethanol, dried under vacuum, and then used in a new reaction. It was found to be reusable for at least four cycles with comparably good results (entry 19), showing the stability of O-MoS_2 (Figure 8).

Two reaction routes for nitrobenzene reduction are widely accepted: the direct route and the condensation route (Scheme 1) [27,58,59]. The condensation route involves an azobenzene intermediate. When azobenzene (0.25 mmol) was used as reactant, O-MoS_2 offered 12.5% conversion at 130 °C in 3 h. The

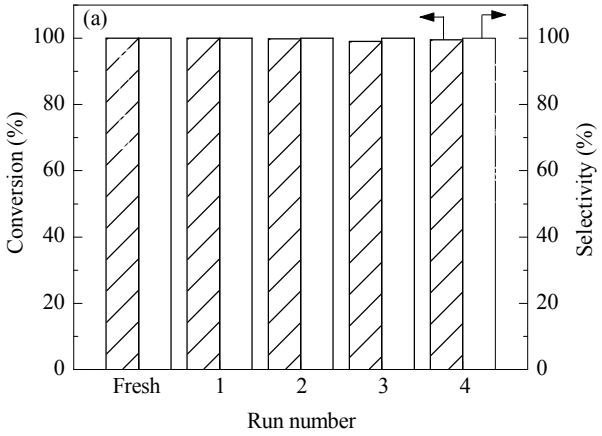

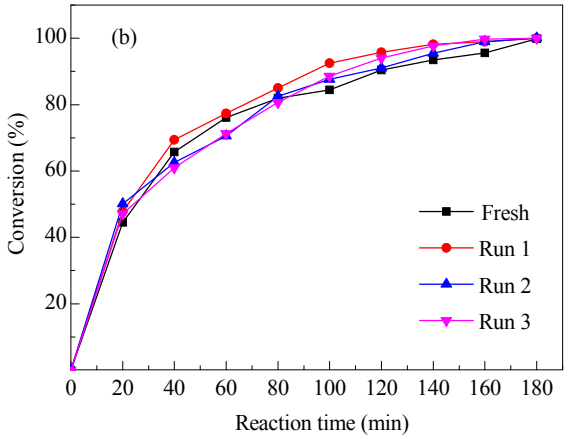

Fig. 8. Reusability of O-MoS_2 in the nitrobenzene reduction reaction. Reaction conditions: nitrobenzene 0.5 mmol, $HCOONH_4$ 3.0 mmol, H_2O 2.5 mL, O-MoS_2 20 mg, Ar, 130 °C, 3 h.

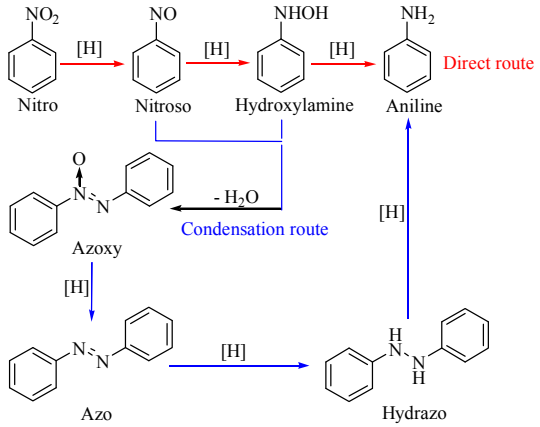

Scheme 1. Reaction network of the nitrobenzene reduction.

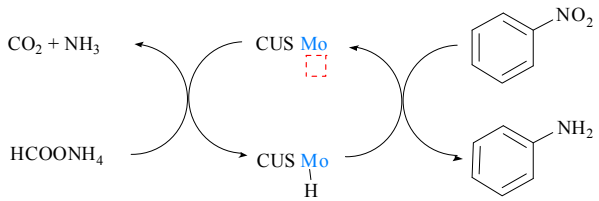

Scheme 2. Possible mechanism of nitrobenzene reduction over the CUS Mo sites on the surface of the O-MoS_2.

conversion of $PhNO_2$ over O-MoS_2 was 7 times greater than the azobenzene conversion. Based on the characterization of the catalyst, we believe that the reaction occurred mainly via the direct route with the following mechanism (Scheme 2): (i) $HCOONH_4$ initially adsorbs on the CUS Mo site and generates a Mo-formate intermediate; (ii) the Mo-formate intermediate transforms to molybdenum hydride (Mo–H) via a β-hydride elimination [28,36,60], simultaneously releasing a CO_2; (iii) finally, the nitro-group is hydrogenated by the Mo–H, and the CUS Mo site is restored to its initial state for the next cycle.

We then explored the substrate scope. *p*-Chloroaniline was obtained in >99% GC yield without dehalogenation (Table 3, entry 1). The nitroarenes with –OH, $–CH_3$, $–COCH_3$ and $–OCH_3$ substituents are only slightly soluble in water, so 0.5 wt% of cetyltrimethyl ammonium bromide (CTAB) relative to the solvent mass was added. By doing so, these nitroarenes were converted to the corresponding arylamines in >99% yield without affecting these functional groups (entries 2–5). The isolated yields of *p*-chloroaniline and *p*-acetylaniline were 92.1% and 87.2%, respectively. Moreover, multiamino aromatic compounds could also be efficiently and selectively produced via the chemoselective reduction of the corresponding nitroarenes or nitroarene (entries 6 and 7). Notably, O-MoS_2 efficiently catalyzed the reduction of a heterocyclic nitroarene to an amine (entry 8). However, it was inactive for the reduction of olefin, alkyne, and carbonyl compounds (entries 10–12) with $HCOONH_4$ at 130 °C. Additionally, 2H-MoS_2 remained catalytically inert in the aqueous solution with CTAB (entry 9).

Table 3
Scope of the reduction reaction with ammonium formate in aqueous solution [a].

Entry	Substrate	Product	GC yield (%)
1[b]	4-Cl-$PhNO_2$	4-Cl-$PhNH_2$	99 (92.1)
2	4-HO-$PhNO_2$	4-HO-$PhNH_2$	>99
3	4-CH_3-$PhNO_2$	4-CH_3-$PhNH_2$	>99
4	4-CH_3CO-$PhNO_2$	4-CH_3CO-$PhNH_2$	99 (87.2)
5	4-CH_3O-$PhNO_2$	4-CH_3O-$PhNH_2$	>99
6	4-H_2N-$PhNO_2$	4-H_2N-$PhNH_2$	>99
7	3-NO_2-$PhNO_2$	3-NH_2-$PhNH_2$	>99
8	5-NO_2-indole	5-NH_2-indole	80.6
9[c]	$PhNO_2$	$PhNH_2$	0
10	Ph-CH=CH_2	Ph-C_2H_5	0
11	Ph-C≡CH	Ph-CH=CH_2	0
12	4-$(CH_3)_2N$-Ph-CHO	4-$(CH_3)_2N$-Ph-CH_3	0.8

[a] Reaction conditions: Substrate 0.5 mmol, H_2O 3.0 mL contains 0.5 wt% of CTAB, $HCOONH_4$ 3.6 mmol, O-MoS_2 20 mg, 130 °C, Ar, 6 h.
[b] No CTAB, 3 h. [c] 2H-MoS_2 20 mg, with CTAB, 3 h.

3.3. *Location of CUS Mo sites*

Next, we quantitatively measured the CUS Mo sites using NH_3-TPD (Figure 9). The chemically exfoliated MoS_2 (ceMoS_2) contained more CUS Mo sites (34.8 μmol/g) than 2H-MoS_2 (10.7 μmol/g). In comparison, the amount of CUS Mo sites in O-MoS_2 (226.4 μmol/g) was 7 times greater than that of ceMoS_2. After treatment in Ar at 250 °C, the amount of CUS Mo sites in O-MoS_2-Ar was remarkably decreased to 11.2 μmol/g. This is consistent with the HRTEM observations (Figures 5(f) and 4(h)), which showed that the lattice matrix became ordered after thermal treatment. In turn, the ordered matrix implies a loss of CUS Mo sites and decreased catalytic activity.

We then established a model to elucidate the location of CUS Mo sites. Here, we assumed that the MoS_2 nanosheets had a parallelogram shape and equal edge lengths. The dependence of the edge CUS Mo site ratio (Rn) among the total Mo ions of the MoS_2 on the edge length (Ln) is given in Figure 10. By assuming all edge Mo to be CUS sites, Rn is equal to $(4n-1)/(n^2+2n)$, where n is the number of hexagons at the edge. The CUS Mo site ratio (R) was calculated for each MoS_2 on the basis of one CUS Mo site adsorbing one NH_3, as given in the inset table of Figure 9. According to the formulae Rn = $(4n-1)/(n^2+2n)$ and Ln = $0.315n$, the edge length of O-MoS_2

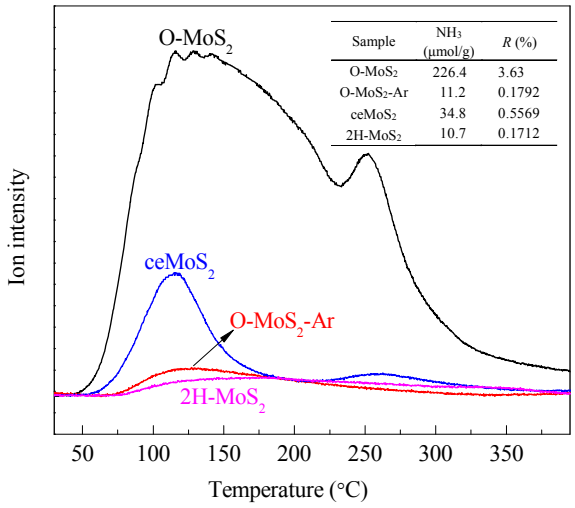

Fig. 9. NH_3-TPD profiles of the MoS_2 materials.

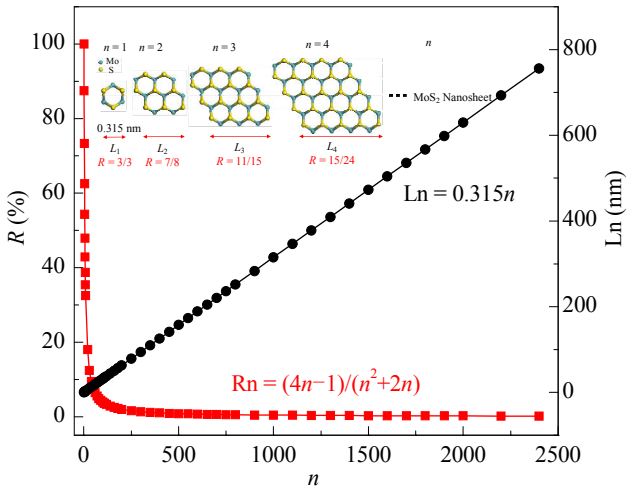

Fig. 10. Ratio model of change in edge sites of MoS_2 with edge length.

should be shorter than 34 nm given that its *R* is 3.63 %. If one CUS Mo site adsorbs two NH_3, the edge length of O-MoS_2 should be 69 nm. Actually, its size was much longer than 200 nm (Figure 5(e)). This inconsistency suggests that only a minor amount of the CUS Mo sites (ca. 5%) existed at the edge, while the majority were located on the distorted basal planes of the O-MoS_2, which is consistent with the HRTEM and NH_3-TPD analyses of O-MoS_2 and O-MoS_2-Ar.

4. Conclusions

We have herein reported a strategy for activating catalytically inert MoS_2 basal planes into highly active locations for the reduction of nitroarenes to arylamines with formate. The active O-MoS_2 was synthesized via incomplete sulfidation and reduction of the molybdate precursor ($[Mo_7O_{24}]^{6-}$). The deliberately left Mo–O bonds interrupted the growth of MoS_2 layers with a perfect lattice, which induced lattice distortion and defects that exposed extra coordinatively unsaturated Mo sites on the basal planes as catalytically active sites, as confirmed by Raman spectroscopy, HRTEM, XPS, EXAFS, and NH_3-TPD. We believe that this MoS_2 synthesis method will broaden the applications of MoS_2 catalysts from traditional high-temperature gas-phase reactions to mild heterogeneous liquid-phase reactions.

References

[1] R. V. Jagadeesh, A. E. Surkus, H. Junge, M. M. Pohl, J. Radnik, J. Rabeah, H. M. Huan, V. Schünemann, A. Brückner, M. Beller, *Science*, **2013**, 342, 1073–1076.
[2] A. Corma, P. Serna, *Science*, **2006**, 313, 332–324.
[3] L. He, L. C. Wang, H. Sun, J. Ni, Y. Cao, H. Y. He, K. N. Ean, *Angew. Chem. Int. Ed.*, **2009**, 48, 9538–9541.
[4] A. Grirrane, A. Corma, H. Garcia, *Science*, **2008**, 322, 1661–1664.
[5] X. Liu, H. Q. Li, S. Ye, Y. M. Liu, H. Y. He, Y. Cao, *Angew. Chem. Int. Ed.*, **2014**, 53, 7624–7628.
[6] R. S. Downing, P. J. Kunkeler, H. van Bekkum, *Catal. Today*, **1997**, 37, 121–136.
[7] M. Pietrowski, *Green Chem.*, **2011**, 13, 1633–1635.
[8] Z. Y. Sun, Y. F. Zhao, Y. Xie, R. T. Tao, H. Y. Zhang, C. L. Huang, Z. M. Liu, *Green Chem.*, **2010**, 12, 1007–1011.
[9] H. S. Wei, X. Y. Liu, A. Q. Wang, L. L. Zhang, B. T. Qiao, X. F. Yang, Y. Q. Huang, S. Miao, J. Y. Liu, T. Zhang, *Nat. Commun.*, **2014**, 5, 5634.
[10] A. Corma, C. González-Arellano, M. Iglesias, F. Sánchez, *Appl. Catal. A*, **2009**, 356, 99–102.
[11] A. Corma, P. Serna, H. García, *J. Am. Chem. Soc.*, **2007**, 129, 6358–6359.
[12] T. Fu, P. Hu, T. Wang, Z. Dong, N. H. Xue, L. M. Peng, X. F. Guo, W. P. Ding, *Chin. J. Catal.*, **2015**, 36, 2030–2035.
[13] J. R. Li, X. H. Li, Y. Ding, P. Wu, *Chin. J. Catal.*, **2015**, 36, 1995–2003.
[14] K. I. Shimizu, Y. Miyamoto, A. Satsuma, *J. Catal.*, **2010**, 270, 86–94.
[15] Y. M. Lu, H. Z. Zhu, W. G. Li, B. Hu, S. H. Yu, *J. Mater. Chem. A*, **2013**, 1, 3783–3788.
[16] X. F. Yang, A. Q. Wang, B. T. Qiao, J. Li, J. Y. Liu, T. Zhang, *Acc. Chem. Res.*, **2013**, 46, 1740–1748.
[17] S. F. Cai, H. H. Duan, H. P. Rong, D. S. Wang, L. S. Li, W. He, Y. D. Li, *ACS Catal.*, **2013**, 3, 608–612.
[18] H. S. Wei, X. Wei, X. F. Yang, G. Z. Yin, A. Q. Wang, X. Y. Liu, Y. Q. Huang, T. Zhang, *Chin. J. Catal.*, **2015**, 36, 160–167.

Graphical Abstract

Chin. J. Catal., 2016, 37: 1569–1577 doi: 10.1016/S1872-2067(16)62504-4

Chemoselective transfer hydrogenation to nitroarenes mediated by oxygen-implanted MoS_2

Chaofeng Zhang, Xu Wang, Mingrun Li, Zhixin Zhang, Yehong Wang, Rui Si, Feng Wang *
Dalian Institute of Chemical Physics, Chinese Academy of Sciences; Shanghai Institute of Applied Physics, Chinese Academy of Sciences; University of Chinese Academy of Sciences

We present an efficient approach for the chemoselective synthesis of arylamines from nitroarenes and formate over an oxygen-implanted MoS_2 catalyst (O-MoS_2). The O-MoS_2 was prepared by incomplete sulfidation and reduction of the ammonium molybdate precursor. O-MoS_2 with abundant CUS Mo sites efficiently catalyzed the chemoselective reduction of nitroarenes to arylamines.

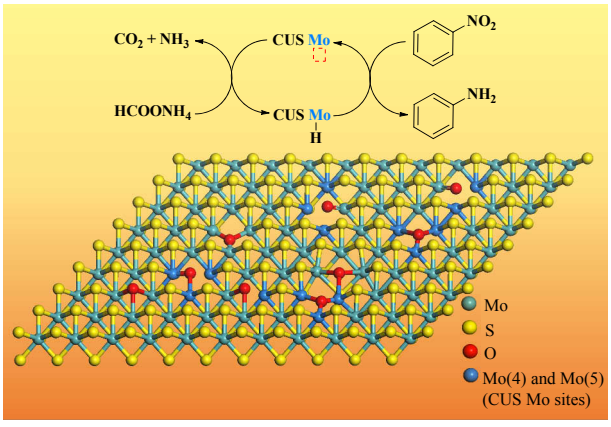

[19] S. P. Jian, Y. W. Li, *Chin. J. Catal.*, **2016**, 37, 91–97.
[20] M. Boronat, P. Concepcion, A. Corma, S. Gonzalez, F. Illas, P. Serna, *J. Am. Chem. Soc.*, **2007**, 129, 16230–16237.
[21] T. Mitsudome, Y. Mikami, M. Matoba, T. Mizugaki, K. Jitsukawa, K. Kaneda, *Angew. Chem. Int. Ed.*, **2012**, 51, 136–139.
[22] A. Noujima, T. Mitsudome, T. Mizugaki, K. Jitsukawa, K. Kaneda, *Angew. Chem. Int. Ed.*, **2011**, 50, 2986–2989.
[23] P. S. Kumbhar, J. Sanchez-Valente, F. Figueras, *Tetrahedron Lett.*, **1998**, 39, 2573–2574.
[24] Q. X. Shi, R. W. Lu, K. Jin, Z. X. Zhang, D. F. Zhao, *Green Chem.*, **2006**, 8, 868–870.
[25] D. Cantillo, M. Baghbanzadeh, C. O. Kappe, *Angew. Chem. Int. Ed.*, **2012**, 51, 10190–10193.
[26] F. A. Westerhaus, R. V. Jagadeesh, G. Wienhöfer, M. M. Pohl, J. Radnik, A. E. Surkus, J. Rabeah, K. Junge, H. Junge, M. Nielsen, A. Brückner, M. Beller, *Nat. Chem.*, **2013**, 5, 537–543.
[27] H. Z. Zhu, Y. M. Lu, F. J. Fan, S. H. Yu, *Nanoscale*, **2013**, 5, 7219–7223.
[28] C. F. Zhang, J. M. Lu, M. R. Li, Y. H. Wang, Z. Zhang, H. J. Chen, F. Wang, *Green Chem.*, **2016**, 18, 2435–2442.
[29] H. Y. Zhou, L. Shi, Q. Sun, *Chin. J. Catal.*, **2012**, 33, 1463–1469.
[30] Z. K. Zhao, H. L. Yang, Y. Li, X. W. Guo, *Green Chem.*, **2014**, 16, 1274–1281.
[31] A. Boddien, F. Gartner, C. Federsel, P. Sponholz, D. Mellmann, R. Jackstell, H. Junge, M. Beller, *Angew. Chem. Int. Ed.*, **2011**, 50, 6411–6414.
[32] X. Liu, S. S. Li, Y. M. Liu, Y. Cao, *Chin. J. Catal.*, **2015**, 36, 1461–1475.
[33] R. V. Jagadeesh, D. Banerjee, P. B. Arockiam, H. Junge, K. Junge, M. M. Pohl, J. Radnik, A. Brückner, M. Beller, *Green Chem.*, **2015**, 17, 898–902.
[34] A. Saha, B. Ranu, *J. Org. Chem.*, **2008**, 73, 6867–6870.
[35] D. C. Gowda, A. S. P. Gowda, A. R. Baba, S. Gowda, *Synth. Commun.*, **2000**, 30, 2889–2895.
[36] I. Sorribes, G. Wienhofer, C. Vicent, K. Junge, R. Llusar, M. Beller, *Angew. Chem. Int. Ed.*, **2012**, 51, 7794–7798.
[37] T. F. Jaramillo, K. P. Jorgensen, J. Bonde, J. H. Nielsen, S. Horch, I. Chorkendorff, *Science*, **2007**, 317, 100–102.
[38] H. I. Karunadasa, E. Montalvo, Y. J. Sun, M. Majda, J. R. Long, C. J. Chang, *Science*, **2012**, 335, 698–702.
[39] J. Kibsgaard, Z. B. Chen, B. N. Reinecke, T. F. Jaramillo, *Nat. Mater.*, **2012**, 11, 963–969.
[40] R. J. Smith, P. J. King, M. Lotya, C. Wirtz, U. Khan, S. De, A. O'Neill, G. S. Duesberg, J. C. Grunlan, G. Moriarty, J. Chen, J. Z. Wang, A. I. Minett, V. Nicolosi, J. N. Coleman, *Adv. Mater.*, **2011**, 23, 3944–3948.
[41] Z. Y. Zeng, T. Sun, J. X. Zhu, X. Huang, Z. Y. Yin, G. Lu, Z. X. Fan, Q. Y. Yan, H. H. Hng, H. Zhang, *Angew. Chem. Int. Ed.*, **2012**, 51, 9052–9056.
[42] K. G. Zhou, N. N. Mao, H. X. Wang, Y. Peng, H. L. Zhang, *Angew. Chem. Int. Ed.*, **2011**, 50, 10839–10842.
[43] R. Tokarz-Sobieraj, R. Grybos, M. Witko, *Appl. Catal., A*, **2011**, 391, 137–143.
[44] B. Radisavljevic, A. Radenovic, J. Brivio, V. Giacometti, A. Kis, *Nat. Nanotech.*, **2011**, 6, 147–150.
[45] J. F. Xie, J. J. Zhang, S. Li, F. Grote, X. D. Zhang, H. Zhang, R. X. Wang, Y. Lei, B. C. Pan, Y. Xie, *J. Am. Chem. Soc.*, **2013**, 135, 17881–17888.
[46] J. F. Xie, H. Zhang, S. Li, R. X. Wang, X. Sun, M. Zhou, J. F. Zhou, X. W. Lou, Y. Xie, *Adv. Mater.*, **2013**, 25, 5807–5813.
[47] J. Deng, H. B. Li, J. P. Xiao, Y.C. Tu, D. H. Deng, H. X. Yang, H. F. Tian, J. Q. Li, P. J. Ren, X. H. Bao, *Energy Environ. Sci.*, **2015**, 8, 1594–1601.
[48] Q. F. Gong, L. Cheng, C. H. Liu, M. Zhang, Q. L. Feng, H. L. Ye, M. Zeng, L. M. Xie, Z. Liu, Y. G. Li, *ACS Catal.*, **2015**, 5, 2213–2219.
[49] S. S. Chou, B. Kaehr, J. Kim, B. M. Foley, M. De, P. E. Hopkins, J. X. Huang, C. J. Brinker, V. P. Dravid, *Angew. Chem. Int. Ed.*, **2013**, 52, 4160–4164.
[50] Y. M. Sun, X. L. Hu, W. Luo, Y. H. Huang, *ACS Nano*, **2011**, 5, 7100–7107.
[51] C. Lee, H. Yan, L. E. Brus, T. F. Heinz, J. Hone, S. Ryu, *ACS Nano*, **2010**, 4, 2695–2700.
[52] H. Li, Q. Zhang, C. C. R. Yap, B. K. Tay, T. H. T. Edwin, A. Olivier, D. Baillargeat, *Adv. Funct. Mater.*, **2012**, 22, 1385–1390.
[53] L. Seguin, M. Figlarz, R. Cavagnat, J. C. Lassègues, *Spectrochim. Acta A*, **1995**, 51, 1323–1344.
[54] X. G. Guo, G. Z. Fang, G. Li, H. Ma, H. J. Fan, L. Yu, C. Ma, X. Wu, D. H. Deng, M. M. Wei, D. L. Tan, R. Si, S. Zhang, J. Q. Li, L. T. Sun, Z. C. Tang, X. L. Pan, X. H. Bao, *Science*, **2014**, 344, 616–619.
[55] J. Ke, W. Zhu, Y. Y. Jiang, R. Si, Y. J. Wang, S. C. Li, C. H. Jin, H. C. Liu, W. G. Song, C. H. Yan, Y. W. Zhang, *ACS Catal.*, **2015**, 5, 5164–5173.
[56] W. W. Wang, P. P. Du, S. H. Zou, H. Y. He, R. X. Wang, Z. Jin, S. Shi, Y. Y. Huang, R. Si, Q. S. Song, C. J. Jia, C. H. Yan, *ACS Catal.*, **2015**, 5, 2088–2099.
[57] Q. Y. Bi, X. L. Du, Y. M. Liu, Y. Cao, H. Y. He, K. N. Fan, *J. Am. Chem. Soc.*, **2012**, 134, 8926–8933.
[58] F. Haber, *Z. Elektrochem. Angew. Phys. Chem.*, **1898**, 4, 506–513.
[59] A. Corma, P. Concepcion, P. Serna, *Angew. Chem. Int. Ed.*, **2007**, 46, 7266–7269.
[60] A. Boddien, D. Mellmann, F. Gärtner, R. Jackstell, H. Junge, P. J. Dyson, G. Laurenczy, R. Ludwig, M. Beller, *Science*, **2011**, 333, 1733–1736.

Page numbers refer to the contents in the print version, which include both the English version and extended Chinese abstract of the paper. The online version only has the English version. The pages with the extended Chinese abstract are only available in the print version.